Time-dependent modeling of resonant-tunneling diodes from direct solution of the Schrödinger equation

R. K. Mains and G. I. Haddad
Center for High-Frequency Microelectronics, Department of Electrical Engineering and Computer Science, The University of Michigan, Ann Arbor, Michigan 48109

(Received 10 February 1988; accepted for publication 21 June 1988)

Numerical solution of the time-dependent Schrödinger equation for resonant-tunneling diodes has been impeded by the difficulty in handling open-system boundary conditions. This paper presents a boundary condition method to simulate the interaction with ideal particle reservoirs at the device boundaries. A switching transient is calculated where the device is switched from the peak current state to the valley current state. In addition, this method was used to develop a small-signal analysis of resonant-tunneling diodes. Results for the small-signal equivalent circuit of a particular device versus frequency are presented.

I. INTRODUCTION

Transient and small-signal behavior of resonant-tunneling diodes has previously been calculated using the Wigner function approach.[1–3] However, due to the numerical problems presented by the solution of the Wigner function equations,[4] it is desirable to obtain direct solutions of the time-dependent Schrödinger equation for comparison. A formalism for solving the time-dependent problem has been presented[5] and a first-order calculation of the response to an applied sinusoidal voltage has previously been carried out.[6] This paper presents an alternative approach, where the time-dependent Schrödinger equation is solved numerically using finite-difference techniques.

Although the time-dependent Schrödinger equation is readily solved numerically for the case where ψ may be set to zero at the boundaries of the simulation,[7] the open nature of the semiconductor device problem requires the formulation of nonzero boundary conditions to model the interaction of the device with particle reservoirs at the contacts, for both the time-independent and time-dependent case.[1] The implementation of this type of boundary condition for the time-dependent problem proves to be a formidable task.

In this paper, boundary conditions are imposed which model to first-order plane waves of constant amplitude incident at the contacts, weighted over the thermal equilibrium distribution function, and waves with modulated amplitude and phase exiting the contacts without reflection. This boundary condition scheme introduces irreversibility in the problem and thereby allows stable, steady-state solutions to be obtained, as well as transient solutions.

The same boundary conditions have also been implemented in a small-signal device analysis, which determines the device conductance and susceptance as functions of frequency. This information may be used to estimate the power generation capability of the device.[3]

II. BASIC SIMULATION METHOD

The method used is that of quantum statistical mechanics,[8] where the system is regarded as a noncoherent superposition of states ψ_i with associated probabilities p_i. The states ψ_i are assumed to be uncorrelated. The set ψ_i is chosen to be the states having constant-amplitude plane waves incident from the left and right, along with associated reflected and transmitted waves. The reflected and transmitted components develop with time as a result of the simulation. At any point in space and time, the electron concentration $n(x,t)$ and the electron current density $J_n(x,t)$ are calculated from

$$n(x,t) = \sum_i p_i \psi_i^*(x,t)\psi_i(x,t) , \tag{1}$$

and

$$J_n(x,t) = \frac{-q\hbar}{m^*} \sum_i p_i \mathrm{Im}\left(\psi_i^*(x,t)\frac{\partial \psi_i(x,t)}{\partial x}\right), \tag{2}$$

where q, the electronic charge in Eq. (2), is a positive quantity. This method is a one-electron picture, where many-body effects such as wave function antisymmetrization are not included. Also, the self-consistent field has not yet been included in this approach.

The initial condition for the time-dependent program is a static solution of the time-independent Schrödinger equation. This is obtained using a recursive algorithm,[1] where a plane-wave boundary condition is set at the outflow point and the solution is stepped through to the inflow boundary, using the tridiagonal form of the Schrödinger equation. The solution for each wave vector k_i is then normalized so that the resulting incident plane wave corresponds to the flux from a particle reservoir at thermal equilibrium:

$$p_i = \frac{m^* k_B T \Delta k}{2\pi^2 \hbar^2} \log\left(1 + e^{[E_F - \hbar^2 k_i^2/(2m^*)]/k_B T}\right), \tag{3}$$

where Δk is the discretization in k space, and E_F the Fermi level in the contact. Equation (3) is obtained by integrating the Fermi–Dirac distribution over transverse momenta.[1]

III. FINITE-DIFFERENCE NUMERICAL METHOD

To obtain the initial condition from the time-independent Schrödinger equation, the tridiagonal form is used which results in the following finite-difference equation:

$$\psi_{i+1} = \left(2 + \frac{2m^*\Delta x^2}{\hbar^2}(V_i' - E)\right)\psi_i - \psi_{i-1} , \tag{4}$$

where the subscripts in (4) indicate the space step, and

 0021-8979/88/193564-06$02.40

where the top or bottom sign is chosen depending on whether the direction of advancement is to the right or left, respectively. In Eq. (4), E is the energy of the eigenstate referenced with respect to the potential at the inflow boundary for that state, so that

$$E = \hbar^2 k^2 / 2m^* , \tag{5}$$

and V' is the potential energy also referenced to the potential at the inflow point, so that

$$V'(x) = V(x) - V(x_{\min}) \tag{6}$$

for states incident at the left-hand boundary, and

$$V'(x) = V(x) - V(x_{\max}) \tag{7}$$

for states incident from the right.

For the time-dependent equation, a half-implicit numerical method is used which is second-order accurate and preserves the normalization of the wave functions.[7] The discrete form at space point j is

$$\left(\frac{1}{2}\right)\psi^f_{j-1} + \left(i\frac{2m^*\Delta x^2}{\hbar\Delta t} - 1 - \frac{m^* V'_j \Delta x^2}{\hbar^2}\right)\psi^f_j + \left(\frac{1}{2}\right) \times \psi^f_{j+1} = \frac{-1}{2}(\psi_{j+1} + \psi_{j-1}) + \left(i\frac{2m^*\Delta x^2}{\hbar\Delta t} + 1 + \frac{m^* V'_j \Delta x^2}{\hbar^2}\right)\psi_j . \tag{8}$$

In this equation, the superscript f denotes a quantity at the future time, $t + \Delta t$. This discretization leads to a tridiagonal matrix which can be efficiently solved using Gaussian elimination.[9]

Once ψ is known, the electron concentration and current density are numerically obtained from

$$n_j = \sum_i p_i \psi^*_{ij} \psi_{ij} , \tag{9}$$

and

$$J_{nj} = \frac{-q\hbar}{m^*} \sum_i p_i \operatorname{Im}\left(\psi^*_{ij} \frac{\psi_{i(j+1)} - \psi_{i(j-1)}}{2\Delta x}\right), \tag{10}$$

where j indicates the space step. It can be shown that this finite difference expression maintains current continuity and reduces to constant current under static conditions.

IV. BOUNDARY CONDITIONS FOR THE TIME-DEPENDENT ANALYSIS

In solving the tridiagonal matrix of Eq. (8), boundary conditions must be specified at the left and right simulation boundaries. It is desirable to set boundary conditions at the inflow point which correspond to incident plane waves of constant amplitude, to model the incident flux of carriers from particle reservoirs. However, at the inflow point there also exists a reflected wave, whose characteristics are not known until the simulation develops. Therefore, the boundary condition should also minimize reflection of this wave at the boundary, to model particles leaving the simulation region. In this manner irreversibility is introduced, since the system loses memory of particles that have exited from the boundary, while the incident distribution is unaffected by these particles.

The approach taken here is to assume that at $t = 0$ (time is redefined to reference zero at the beginning of each time step), the wave function at the boundary is given by (for the case of particles incident from the left)

$$\psi = Ae^{ikx} + B(x)e^{-ikx} , \tag{11}$$

where ψ here represents only a single incident state, ψ_i, in the ensemble. It is assumed that A is a constant to model the interaction with the reservoir, however, the envelope function of the reflected wave, $B(x)$, is allowed to vary with x, since, in general, the amplitude of the wave reflected from the device will vary with space and time. If the further assumption is made that to a good approximation the variation of $B(x)$ near the boundary may be regarded as linear, then the time-dependent Schrödinger equation at the boundary becomes

$$i\hbar\frac{\partial\psi}{\partial t} = \frac{\hbar^2 k^2}{2m^*}\psi + i\frac{\hbar^2 k}{m^*}\frac{\partial B(x)}{\partial x}e^{-ikx} , \tag{12}$$

where the potential energy at the boundary does not appear since V' is zero at the inflow boundary. The solution for ψ at the future time may be approximately written as

$$\psi(t = \Delta t) \approx \psi(t = 0)e^{-i(E/\hbar)\Delta t} + \frac{\hbar k}{m^*}\frac{\partial B(x)}{\partial x}e^{-ikx}\Delta t . \tag{13}$$

In this equation, the first term on the right gives the time advancement expected for an energy eigenstate, for which $B(x)$ would be constant. The second term gives the modification of ψ due to the local variation of the reflected wave. Since this is an explicit time advancement for the second term, this time advancement scheme can only be used provided the time step Δt does not exceed a maximum limiting value. For the results presented here, a maximum value of $\Delta t = 2\times 10^{-16}$ s was found to sufficiently eliminate reflections at the boundary while still maintaining numerical stability. It may be possible to implement an iterative version of Eq. (13) for which larger time steps may be taken, although this has not yet been attempted.

At the outflow point, only a transmitted wave exiting the boundary is expected, however the amplitude of this wave will, in general, not be constant. Therefore at the outflow, the wave function is assumed to be

$$\psi = C(x)e^{ik_0 x} , \tag{14}$$

where the wave vector k_0 differs from k appearing in Eq. (11) as follows (again for the case of an incident wave from the left):

$$k_0 = \sqrt{2m^*[E - V'(x_{\max})]}/\hbar . \tag{15}$$

Again assuming that to a good approximation $C(x)$ varies linearly, the time-dependent Schrödinger equation may be approximately solved to give the update:

$$\psi(t = \Delta t) \approx \psi(t = 0)e^{-i(E/\hbar)\Delta t} - \frac{\hbar k_0}{m^*}\frac{\partial C(x)}{\partial x}e^{ik_0 x}\Delta t . \tag{16}$$

Note from Eq. (15) that for applied bias with $V(x_{\max}) > V(x_{\min})$, k_0 is imaginary and the waves at the outflow boundary are evanescent waves. In practice, using Eq. (16) to set boundary conditions for evanescent modes causes numerical problems, so that Eq. (16) was used only

for modes with traveling waves at the outflow points. For substantial applied bias, the evanescent modes do not contribute to current flow, and for the simulations presented here these states were assumed not to change from the equilibrium wave functions given by the time-independent solution. Further work needs to be done to successfully implement boundary conditions of the type in Eq. (16) for these waves, in order to study transient behavior where the bias voltage approaches zero.

The boundary updates given by Eqs. (13) and (16) are used to set Dirichlet boundary conditions on the tridiagonal system of Eq. (8). It is seen that in order to use these expressions, $\partial B(x)/\partial x$ and $\partial C(x)/\partial x$ must be determined. At the inflow point, the time variation of the incident wave $\psi_{\rm inc}$ is known to be

$$\psi_{\rm inc}(x,t) = Ae^{ikx}e^{-i(E/\hbar)t}. \tag{17}$$

At any time t, the reflected wave at the first two mesh points is determined from

$$\psi_r(x_{\rm min}) = \psi(x_{\rm min}) - \psi_{\rm inc}(x_{\rm min}),$$
$$\psi_r(x_{\rm min}+\Delta x) = \psi(x_{\rm min}+\Delta x) - \psi_{\rm inc}(x_{\rm min}+\Delta x). \tag{18}$$

The values of $B(x)$ at the first two points are then determined from

$$B(x_{\rm min}) = \psi_r(x_{\rm min})e^{ikx_{\rm min}},$$
$$B(x_{\rm min}+\Delta x) = \psi_r(x_{\rm min}+\Delta x)e^{ik(x_{\rm min}+\Delta x)}. \tag{19}$$

The values obtained from (19) are then used to approximate the gradient as follows:

$$\frac{\partial B(x)}{\partial x} \approx \frac{B(x_{\rm min}+\Delta x) - B(x_{\rm min})}{\Delta x}. \tag{20}$$

A similar procedure is used to determine $\partial C/\partial x$, except in this case it is not necessary to subtract out the incident wave component.

V. SMALL-SIGNAL ANALYSIS

The boundary conditions of the previous section were also implemented in a small-signal analysis. In the following discussion, a single wave function of the set ψ_i is implied. It is assumed that each wave function, multiplied by the appropriate eigenstate phase factor, takes the following form:

$$\psi e^{i(E/\hbar)t} = \psi_{\rm dc}(x) + \tilde{\psi}(x)e^{i\omega t}, \tag{21}$$

where a small-signal applied potential of frequency ω is presumed. In this equation, $\psi_{\rm dc}$ is the wave function obtained from the time-independent analysis, and $\tilde{\psi}$ is the deviation of the wave function resulting from the applied small-signal potential. This form ensures that quantities such as local current density and carrier concentration have the proper harmonic dependence.

Substituting the form of the wave function given in (21) into the time-dependent Schrödinger equation, canceling out the dc terms, and retaining small-signal terms to first order only, the following equation for $\tilde{\psi}$ is obtained:

$$(E-\hbar\omega)\tilde{\psi}(x) = \left(\frac{-\hbar^2}{2m^*}\frac{\partial^2}{\partial x^2} + V_{\rm dc}(x)\right) \times \tilde{\psi}(x) + \tilde{V}(x)\psi_{\rm dc}(x), \tag{22}$$

where in (22) a potential energy of the following form is assumed:

$$V(x,t) = V_{\rm dc}(x) + \tilde{V}(x)e^{i\omega t}. \tag{23}$$

Note from (23) that the assumed potential is not real. Therefore, two calculations are required to determine the small-signal response, one for positive ω and a conjugate calculation for negative ω, after which the results are added together. Therefore, $\psi_{\rm ss}$ is the sum of two terms:

$$\psi_{\rm ss}(x,t) = \tfrac{1}{2}[\tilde{\psi}_+(x)e^{i\omega t} + \tilde{\psi}_-(x)e^{-i\omega t}], \tag{24}$$

where $\tilde{\psi}_+$ and $\tilde{\psi}_-$ result from the conjugate calculations with positive and negative ω, respectively.

The discrete form of Eq. (22) at point j is

$$\tilde{V}_j\psi_{\rm dc}(x_j) = \left(\frac{\hbar^2}{2m^*\Delta x^2}\right)\tilde{\psi}_{j-1} + \left(E-\hbar\omega - \frac{\hbar^2}{m^*\Delta x^2} - V_{\rm dc}(x_j)\right) \times \tilde{\psi}_j + \left(\frac{\hbar^2}{2m^*\Delta x^2}\right)\tilde{\psi}_{j+1}. \tag{25}$$

This discrete equation is also of tridiagonal form and may be solved using the technique of Sec. III. Again, boundary conditions must be set at the left- and right-hand sides. The method of Sec. IV is used, however the expressions are different for the small-signal case. The variation of $B(x)$ and $C(x)$ is now entirely due to the small-signal perturbation, which leads to the following identification at the inflow point, for the positive ω calculation:

$$B(x) = \tilde{\psi}_+(x)e^{i(kx+\omega t)}. \tag{26}$$

The rate of change of ψ at the inflow boundary due to the $B(x)$ variation is then given by (again using the linear approximation)

$$\left.\frac{\partial\psi}{\partial t}\right|_{B(x)} = \frac{\hbar k}{m^*}\frac{\partial B(x)}{\partial x}e^{-i[kx+(E/\hbar)t]} = \frac{\hbar k}{m^*}e^{-i[kx+(E/\hbar)t]} \times \left(ike^{ikx}\tilde{\psi}_+(x) + e^{ikx}\frac{\partial\tilde{\psi}_+(x)}{\partial x}\right)e^{i\omega t}. \tag{27}$$

Substituting this form into the time-dependent Schrödinger equation and canceling out the dc terms yields the following relation at the inflow boundary, for the positive ω calculation:

$$i\left(\omega - \frac{\hbar k^2}{m^*}\right)\tilde{\psi}_+(x) - \frac{\hbar k}{m^*}\frac{\partial\tilde{\psi}_+(x)}{\partial x} = 0. \tag{28}$$

A similar procedure at the outflow leads to the following expression:

$$i\left(\omega - \frac{\hbar k^2}{m^*}\right)\tilde{\psi}_+(x) + \frac{\hbar k}{m^*}\frac{\partial\tilde{\psi}_+(x)}{\partial x} = 0. \tag{29}$$

Equations (28) and (29) are set as mixed boundary conditions on the tridiagonal matrix solution.[9]

Substituting the form of the wave function given in Eq. (21) into the expression for current and canceling out the dc components yields the following expression for the small-signal current density $J_{\rm ss}$ (for a single state):

$$J_{ss} = \frac{-q\hbar}{m^*}\left[\frac{1}{2}\,\mathrm{Im}\left(\psi_{dc}^* \frac{\partial \tilde{\psi}_+}{\partial x}\right)\cos(\omega t) + \frac{1}{2}\,\mathrm{Re}\left(\psi_{dc}^* \frac{\partial \tilde{\psi}_+}{\partial x}\right)\sin(\omega t) + \frac{1}{2}\,\mathrm{Im}\left(\psi_{dc}^* \frac{\partial \tilde{\psi}_-}{\partial x}\right)\cos(\omega t) - \frac{1}{2}\,\mathrm{Re}\left(\psi_{dc}^* \frac{\partial \tilde{\psi}_-}{\partial x}\right)\sin(\omega t)\right.$$
$$\left. + \frac{1}{2}\,\mathrm{Im}\left(\tilde{\psi}_+^* \frac{\partial \psi_{dc}}{\partial x}\right)\cos(\omega t) - \frac{1}{2}\,\mathrm{Re}\left(\tilde{\psi}_+^* \frac{\partial \psi_{dc}}{\partial x}\right)\sin(\omega t) + \frac{1}{2}\,\mathrm{Im}\left(\tilde{\psi}_-^* \frac{\partial \psi_{dc}}{\partial x}\right)\cos(\omega t) + \frac{1}{2}\,\mathrm{Re}\left(\tilde{\psi}_-^* \frac{\partial \psi_{dc}}{\partial x}\right)\sin(\omega t)\right]. \tag{30}$$

In Eq. (30), terms multiplying $\cos(\omega t)$ are in phase with the applied small-signal potential, while terms multiplying $\sin(\omega t)$ are 90° out of phase. The small-signal potential is applied across the barrier and well regions; Eq. (30) is evaluated and averaged over the same region. The ratio of the averaged J_{ss} and the applied small-signal voltage then gives the device admittance per unit area. Since Eq. (30) only takes into account the conduction current, the term ωC is added to the device susceptance to account for displacement current.[3]

VI. RESULTS

The calculations were for a structure for which Wigner function results have previously been obtained.[3] The device is a pseudomorphic $In_{0.53}Ga_{0.47}As$-AlAs structure for which excellent experimental results have been observed.[10] Peak-to-valley ratios of 14 at room temperature and 35 at 77 K have been obtained, with current densities in the range of $(2\text{–}4)\times 10^4$ A/cm^2. For this device, the well width is 45.2 Å, the barrier widths are 22.6 Å, the conduction-band discontinuity is assumed 1.2 eV, and the effective mass used is $m^* = 0.042m_0$. Figure 1 shows the static I-V curve at room temperature calculated using the recursive algorithm for solving the time-independent Schrödinger equation.[1] In the calculation, $N_x = 160$ points in real space and $N_k = 800$ points in k space were used, with $\Delta x = 2.81$ Å and $\Delta k = 1\times 10^6\ \mathrm{m}^{-1}$. This calculation does not include scattering, so that the temperature enters the problem only in the distribution function weighting for incident waves given in Eq. (3). The peak-to-valley ratio for this case is 120, much larger than the experimental value and also larger than the value of 34.7 obtained from the corresponding Wigner function calculations.[3,4] It is believed that the Wigner function calculation is lower due to numerical problems in solving the quantum Liouville equation.[4] It remains to include scattering mechanisms in the Schrödinger equation solution to see how well the room-temperature I-V curves compare with experimental results.

The device was biased at the point $V_{dc} = 0.465$ V, in the middle of the negative conductance region, and the methods of Sec. V were used to calculate the admittance as a function of frequency. Figure 2 shows the calculated device conductance and susceptance based on the conduction current alone; also shown is the ωC displacement current component, assuming that the device capacitance appears across the barrier and well regions, a width of 90.4 Å. Comparison with Wigner function results[3] shows that the maximum magnitude of the negative conductance is greater for the Schrödinger calculation; this is because the slope of the I-V curve in Fig. 1 is greater in the negative conductance region. Also, the negative conductance in Fig. 2 begins to roll off at 100 GHz, whereas the Wigner function result predicts nearly constant negative conductance well into the THz range. Finally, the susceptance in Fig. 2 is inductive, whereas capacitive susceptance had been obtained using the Wigner function.[3] Inductive susceptance is more reasonable physically and has been obtained in another Wigner function calculation.[2] It is not known why the Wigner function calculation of Ref. 3 predicts capacitive susceptance.

Using the methods of Ref. 3, the power generation capability and required device area were estimated assuming 1-Ω circuit matching; the results are presented in Fig. 3. The estimated power is considerably lower than for the Wigner function calculation,[3] since the allowed rf voltage swing in the negative conductance region of Fig. 1 is substantially reduced. Also due to the reduced V_{rf} range, the large-signal efficiency is estimated to be only 5.3%, a factor of 4 smaller than the efficiency predicted from Wigner function simulation.[3]

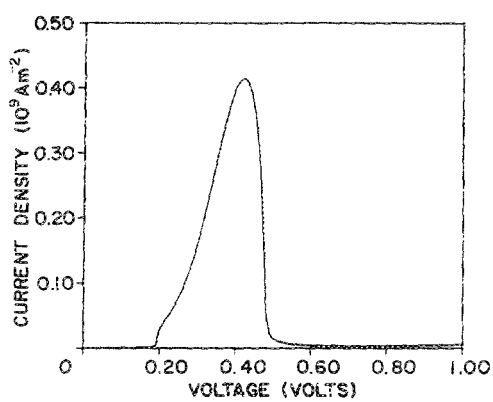

FIG. 1. Static I-V curve at room temperature. Barrier widths = 22.6 Å, well width = 45.2 Å, conduction-band discontinuity = 1.2 eV, $m^* = 0.042m_0$.

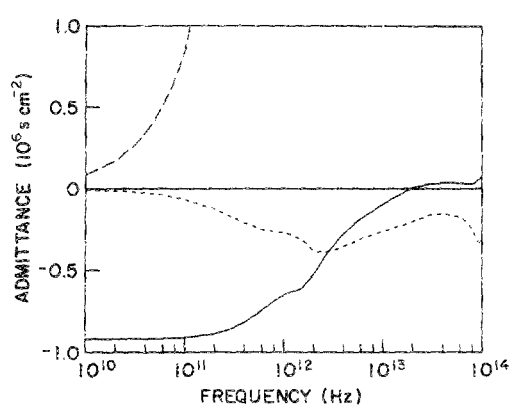

FIG. 2. Small-signal admittance calculated for the dc operating point at $V_{dc} = 0.465$ V in Fig. 1. Solid curve is Re(Y), small dashed curve is Im(Y), large dashed curve is ωC.

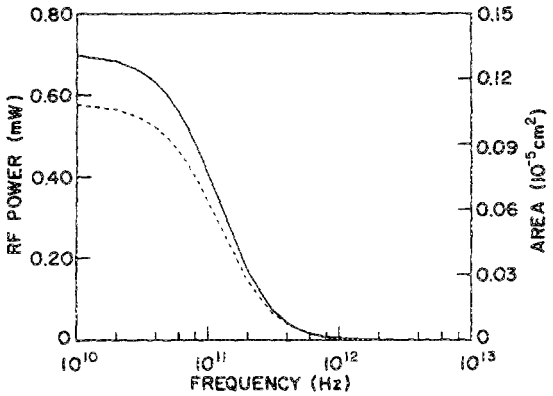

FIG. 3. Estimated power generation (solid) and device area (dashed) for 1-Ω matching based on the small-signal data of Fig. 2 and using $(V_{rf})_{peak} = 37.5$ mV.

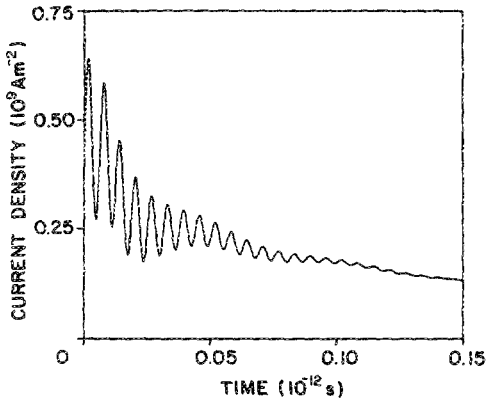

FIG. 5. Initial portion of switching transient for $V_{dc} = 0.42$ V instantaneously switched to $V_{dc} = 0.62$ V at $t = 0$ (current referenced positive to the left in this figure).

The device was next switched from a static solution at $V_{dc} = 0.42$ V, corresponding to the peak current in Fig. 1, to the bias point $V_{dc} = 0.62$ V, in the valley current region. Figure 4 shows the static solution at the peak current point, where the resonant buildup in the well is clearly visible. Figure 5 shows the conduction current averaged over the entire device during the initial 0.15 ps of the resulting transient. The oscillation period corresponds almost exactly to the round-trip transit time of a wave packet centered about the resonant energy within the well. Figure 6 shows the current density within the device at times early in the transient corresponding to positive and negative current oscillations. Figure 7 shows the entire calculated transient, where a long exponential tail is evident after the initial oscillations have disappeared. During this time the resonant buildup of the wave functions within the well is extracted on the right-hand side. Figure 8 shows the carrier concentration and current density at $t = 0.4$ ps, half-way through the transient of Fig. 7. The current on the left-hand side of the device is nearly zero, however the current on the right-hand side of the structure is negative as the remaining resonant wave functions are drained from the well. Figure 9 shows the carrier concentration and current density at the conclusion of the calculation. At this point the current averaged over the entire device is 754 A/cm^2, which has not yet reached the current resulting from the static solution at $V = 0.62$ V of 403 A/cm^2. This is

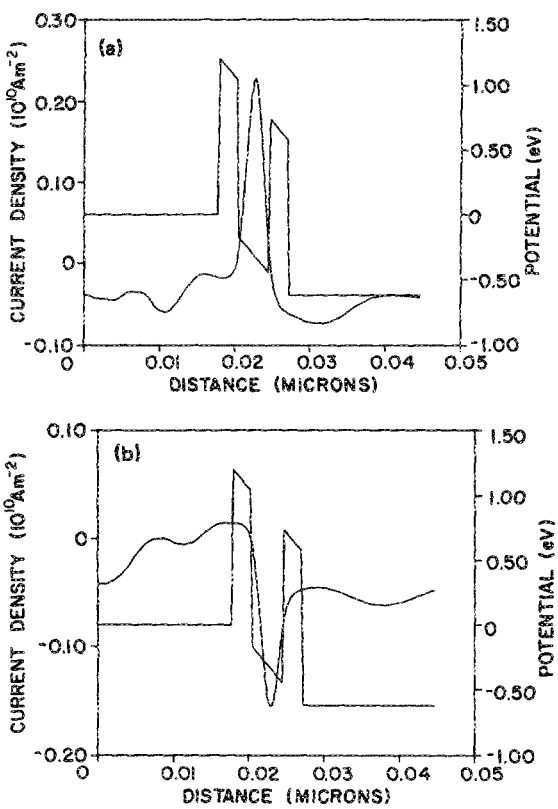

FIG. 6. Current density within the device at (a) $t = 5$ fs and (b) $t = 20$ fs showing points of positive and negative current oscillation.

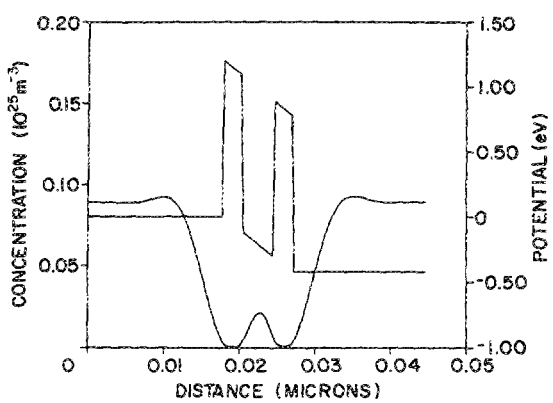

FIG. 4. Static solution at room temperature with $V_{dc} = 0.42$ V, $J_{dc} = 4.16 \times 10^4$ A/cm^2.

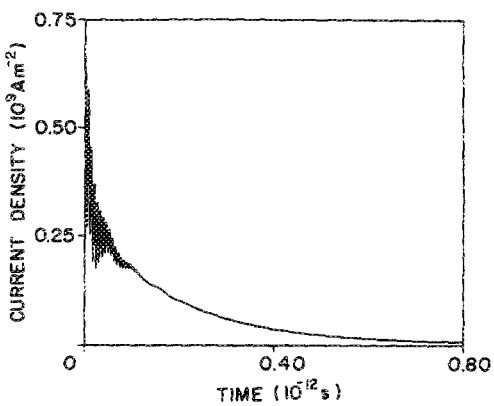

FIG. 7. Entire switching transient from $V_{dc} = 0.42$ to 0.62 V (current referenced positive to the left in this figure).

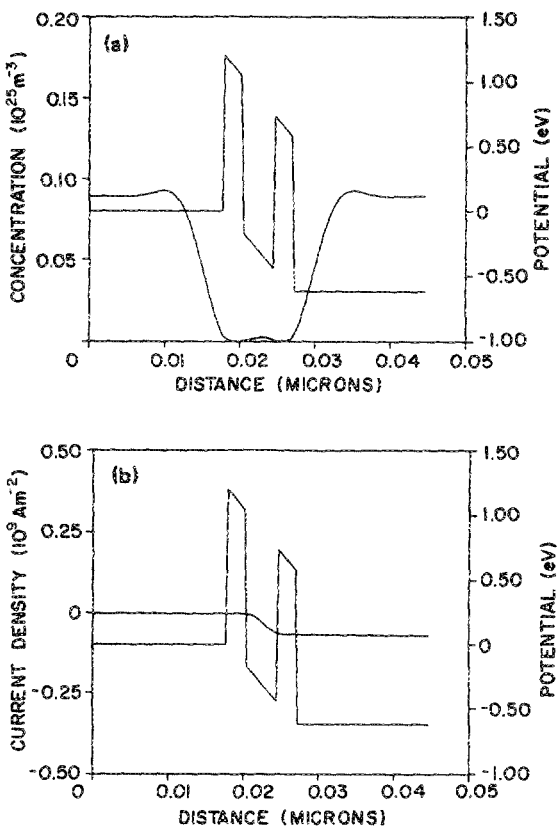

FIG. 8. (a) Carrier concentration and (b) current density within the device at $t = 0.4$ ps half-way through the switching transient.

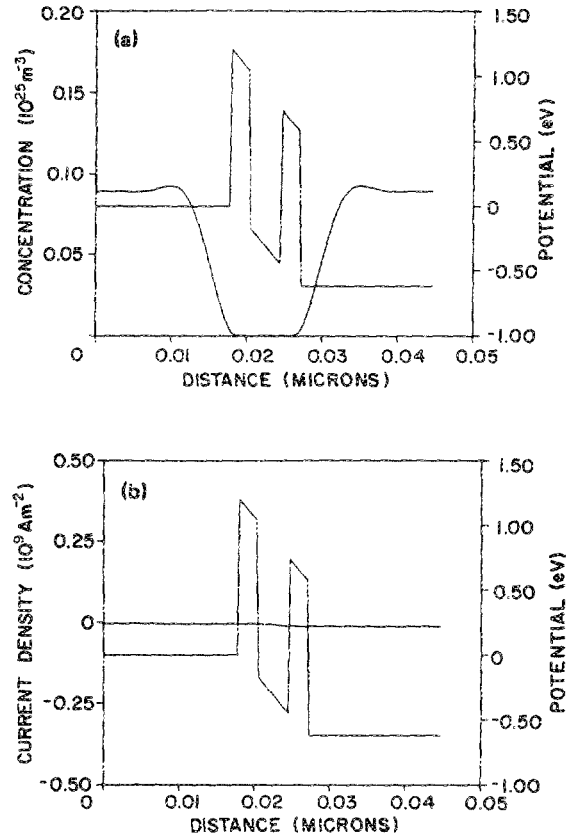

FIG. 9. (a) Carrier concentration and (b) current density within the device at $t = 0.8$ ps at the conclusion of the calculated transient.

because the current density is still slowly decreasing at the conclusion of the calculated transient.

Due to the short intrinsic response time for this device, in practical applications the switching speed will be limited by displacement current required to charge the device capacitance and by external circuit impedance limitations.

VII. CONCLUSIONS

A method of solving the time-dependent Schrödinger equation with boundary conditions modeling the interaction of the device with particle reservoirs at the contacts has been presented. This method is stable provided the time step is not too large. A small-signal analysis based on the same boundary condition treatment has also been presented. Small-signal and switching transient results for a particular resonant-tunneling diode have been shown. A switching time from peak-to-valley current biases of 0.8 ps was calculated. It is believed that this time is on the high end for these devices, since a large conduction-band discontinuity of 1.2 eV was assumed in the calculations. Important differences with previous Wigner function calculations have been noted.

Since scattering mechanisms were not included in this analysis, the influence of such effects as phonon-assisted tunneling has not been evaluated. It is expected that these effects would significantly degrade the peak-to-valley ratio. Work is currently under way to include scattering mechanisms in the simulation.

Future work in this area should include an iterative formulation of the boundary condition scheme, which hopefully will allow larger time steps to be taken in the transient calculations. In addition, work should be done on including evanescent modes in the analysis, since these modes may be important in some transient calculations. Also, it is desirable to include important effects such as scattering and self-consistency to improve agreement of this method with experimental results.

ACKNOWLEDGMENTS

This work was supported by the U.S. Army Research Office under the URI program, Contract No. DAAL03-87-K-0007. The authors wish to thank Dr. William Frensley for suggesting the recursive algorithm for time-independent analysis.

[1] W. R. Frensley, Phys. Rev. B **38**, 1570 (1987).
[2] W. R. Frensley, Appl. Phys. Lett. **51**, 448 (1987).
[3] R. K. Mains and G. I. Haddad (to be published).
[4] R. K. Mains and G. I. Haddad (to be published).
[5] D. D. Coon and H. C. Liu, J. Appl. Phys. **58**, 2230 (1985).
[6] H. C. Liu, Appl. Phys. Lett. **52**, 453 (1988).
[7] A. Goldberg, H. M. Schey, and J. L. Schwartz, Am. J. Phys. **35**, 177 (1967).
[8] R. Balescu, *Equilibrium and Nonequilibrium Statistical Mechanics* (Wiley, New York, 1975).
[9] P. J. Roache, *Computational Fluid Dynamics* (Hermosa, Albuquerque, NM, 1976).
[10] T. Inata, S. Muto, Y. Nakata, S. Sasa, T. Fujii, and S. Hiyamizu, Jpn. J. Appl. Phys. **28**, L1332 (1987).